Fluorescence Investigation of Multiple Partitioning Sites in Aqueous and Reverse Micelles

Kerry K. Karukstis,* April A. Frazier, Christine T. Loftus, and August S. Tuan

Department of Chemistry, Harvey Mudd College, Claremont, California 91711

Received: January 30, 1998; In Final Form: June 8, 1998

Our investigations seek to illustrate the use of fluorescence spectral deconvolution to characterize multiple partitioning sites for aromatic chromophores within aqueous and reverse micelles. The spatial distribution of solutes within micellar systems is dictated by a variety of noncovalent interactions. To probe for multiple partitioning microenvironments, we use the aromatic fluorophore Prodan with its extensive solubility in a range of media and its appreciable spectral sensitivity to the polarity of its surroundings. We conduct a systematic study of the partitioning of Prodan in aqueous micellar systems with anionic, cationic, zwitterionic, and nonionic surfactant headgroups and in reverse micellar systems with both anionic and cationic surfactant headgroups. By deconvoluting the overall Prodan fluorescence emission spectrum into a sum of overlapping Gaussian functions, the principal microenvironments of the Prodan molecules may be ascertained. Fluorescence data are consistent with the location of Prodan in a variety of sites, including partitionings that may be influenced by electrostatic, hydrophobic, dipolar, and cation$-\pi$ interactions in both aqueous and reverse micelles.

Introduction

We have previously demonstrated that the fluorophore Prodan (6-propionyl-2-(dimethylamino)-naphthalene) is a novel and powerful probe of the features of aqueous and reverse micellar systems.[1,2] In particular, Prodan's solubility in a wide-range of solvents[1−3] enables the distribution of this neutral probe into multiple micellar microregions. Furthermore, a fluorescence signal that is simultaneously indicative of multiple locations results as a consequence of both the measurable fluorescence intensity of Prodan in an extensive number of solvents and the sensitivity of the wavelength of maximum emission (λ_{max}) to the polarity of Prodan's environment.[1−3] Deconvolution of the overall Prodan fluorescence emission spectrum into a sum of overlapping Gaussian functions is interpreted to reflect discrete populations of Prodan molecules with surroundings consistent with one of the principal regions of aqueous and reverse micelles. The noncovalent interactions that govern the distribution of solutes within micellar domains include electrostatic interactions, hydrogen bonding, van der Waals or dipole forces, and hydrophobic effects. An increasing recognition of the role of "cation$-\pi$ interactions" in mediating the association of guest molecules in host systems has also been acknowledged.[4−9] In general, an electrostatic interaction of a cation with the large, permanent quadrupole moment of an aromatic π cloud is the major contributor to this binding force.[9−11] In the present study, by using micellar systems with different amphiphilic structures, we generate a varied number of potential partitioning sites with a range of noncovalent interactions that dictate probe distribution. Our systematic investigation illustrates a means of deciphering the complex emission spectra arising from the partitioning of the fluorescence probe Prodan into multiple micellar domains.

Experimental Section

Aqueous Micelle Preparation. The following surfactants were used without further purification: sodium dodecyl sulfate (SDS; Aldrich, >99%); dodecyltrimethylammonium bromide (DTAB; C_nTAB where $n = 12$; Aldrich, 99%), myristyltrimethylammonium bromide (MTAB; C_nTAB where $n = 14$, Aldrich, 99%), cetyltrimethylammonium bromide (CTAB; C_nTAB where $n = 16$, Calbiochem, >99.9%), octadecyltrimethylammonium bromide (OTAB; C_nTAB where $n = 18$, Calbiochem, 99.9%), lauryldimethylamine oxide (LDAO; Calbiochem, 30% (w/w) aqueous solution), polyoxyethylene 8 lauryl ether ($C_{12}E_8$, Sigma), and polyoxyethylene 8 myristyl ether ($C_{14}E_8$, Sigma). We conducted preliminary investigations with varying surfactant concentration in order to select a surfactant concentration above the critical micelle concentration (cmc) value for micelle formation. The fluorescence intensity of Prodan rises sharply above the cmc, reflecting a more nonpolar environment for the fluorophore.[1] Surfactant concentrations ranged from 0 to 18 mM for SDS, 0 to 30 mM for DTAB, 0 to 5.0 mM for MTAB, 0 to 3.0 mM for CTAB, 0 to 0.20 mM for OTAB, 0 to 2.5 mM for LDAO, 0 to 0.40 mM for $C_{12}E_8$, and 0 to 0.10 mM for $C_{14}E_8$. All aqueous solutions were prepared using 18.2 MΩ ultrapure water obtained from a Milli-Q Plus Millipore water filtration system. The pH values of LDAO micellar solutions were adjusted with small amounts of hydrochloric acid or sodium hydroxide solution to achieve a pH range of 5.12−10.45. All solutions were allowed to equilibrate overnight. Surfactant concentrations selected for micellar formation and further fluorescence analysis were 15 mM SDS, 30. mM DTAB, 4.0 mM MTAB, 3.0 mM CTAB, 0.20 mM OTAB, 2.5 mM LDAO, 0.40 mM $C_{12}E_8$, and 0.10 mM $C_{14}E_8$. For counterion studies with SDS and DTAB micelles, aliquots of a concentrated stock solution of NaCl (Aldrich; >99%) were added to micellar solutions prior to Prodan treatment to achieve the desired concentration of NaCl. Surfactant concentrations selected for micellar formation in the presence of NaCl were 4.0 mM SDS for [NaCl] ≤ 0.10 M, 2.0 mM SDS for 0.10 M < [NaCl] ≤ 0.75 M, and 30 mM DTAB for [NaCl] ≤ 0.50 M.

AOT Reverse Micelle Preparation. Spectrophotometric grade *n*-heptane (Aldrich) and sodium bis(2-ethylhexyl)sulfosuccinate (AOT; Sigma, > 99% purity) were used without

* To whom correspondence should be addressed. E-mail address: Kerry_Karukstis@hmc.edu. Fax: (909) 607-7577. Phone: (909) 607-3225.

S1089-5647(98)00955-9 CCC: $15.00
Published on Web 09/17/1998

further purification. Samples were prepared by dissolving appropriate amounts of AOT in heptane and adding specific volumes of Millipore-filtered water to achieve the desired molar ratio of water to AOT (i.e., R = [water]/[AOT]). Final reagent concentrations were 0.20 M AOT and 5 μM Prodan, with R values varying from 2 to 30. Volume additivity was assumed in calculating AOT concentration and water/AOT molar ratios.

DTAB and CTAB Reverse Micelle Preparation. HPLC grade *n*-heptane (Aldrich), 1-hexanol (Aldrich, 98%), dodecyltrimethylammonium bromide (DTAB; Aldrich, 99%), and cetyltrimethylammonium bromide (CTAB; Calbiochem, 99.9%) were used without further purification. Samples were prepared by dissolving appropriate amounts of DTAB and CTAB in heptane and adding specific volumes of the stabilizing cosurfactant 1-hexanol, Millipore-filtered water, and Prodan to achieve the desired composition. Final reagent concentrations were 0.015 M DTAB and CTAB, 10.0% (v/v) 1-hexanol, and 50 μM Prodan, with a molar ratio of water to DTAB (i.e., R = [water]/[DTAB]) varying from 1 to 30 for DTAB and from 10 to 50 for CTAB. Volume additivity was assumed in calculating surfactant concentrations and water/surfactant molar ratios.

Fluorescence Probe. 6-propionyl-2-(dimethylamino)naphthalene (Prodan; Molecular Probes, Eugene, Oregon) was dissolved in dimethyl sulfoxide (DMSO; Aldrich, HPLC grade) to produce a 5 mM stock solution. Prodan (5 μM) was added to micellar solutions prior to fluorescence measurements, with micellar equilibrium and probe partitioning presumed to be established by the absence of any time-dependent variation in Prodan fluorescence. The low concentration of fluorophore was selected (1) to enhance the interaction of micelles and probe by minimizing the amount of "free" Prodan and (2) to ensure a low probability of multiple probe molecules per micelle.

Fluorescence Measurements and Analyses. Fluorescence emission spectra were obtained using a Perkin-Elmer LS-50B fluorescence spectrophotometer. Fluorescence was induced by varying the excitation wavelength in 10-nm increments between 280 and 360 nm, and emission was monitored from 370 to 540 nm. Excitation and emission slit widths were set at 5 nm. While overall Prodan fluorescence intensity varies with excitation wavelength, we observed little variation in spectral shape for all surfactants examined. Except as otherwise noted, the emission spectra presented are those generated with an excitation wavelength of 360 nm (yielding maximum fluorescence intensities). A nonlinear least-squares-fitting routine (PeakFit, Jandel Scientific) was used to deconvolute individual emission spectra into a sum of overlapping Gaussian functions with frequency as the independent variable. All spectra were fit using an iterative Marquardt−Levenberg fitting algorithm to obtain the minimum number of fluorescing components that yielded an r^2 of at least 0.9999 with a random scattering of residuals. The center, amplitude, width, and area of each Gaussian function were characterized.

Results

(a) Resolution of Prodan Fluorescence in SDS (Anionic) Aqueous Micelles. As an example of the enhancement of Prodan fluorescence observed as surfactant concentration is increased above the cmc, Figure 1 illustrates the variation in the maximum Prodan fluorescence intensity (excitation wavelength of 340 nm) as SDS concentration is increased over the range of 0−18 mM. An SDS concentration of 15 mM was selected for further spectral analysis, and deconvolution of the fluorescence emission spectrum yields a single Gaussian component at 505 ± 1 nm (independent of excitation wavelength), as illustrated in Figure 2a. The presence of 0.050 M NaCl in a 4.0 mM SDS micellar solution to reduce the electrostatic repulsions between anionic sulfonate headgroups without a significant change in micellar shape[12] continues to generate a fluorescence spectrum fit by a single Gaussian curve centered at 506 ± 1 nm. Higher salt concentrations that yield cylindrically shaped SDS micelles[12] yield a fluorescence emission spectrum fit by two Gaussian curves, such as shown in Figure 2b with λ_{max} at 501 ± 1 nm and at 431 ± 1 nm for 2 mM SDS in the presence of 0.75 M NaCl. The shorter wavelength component contributes 5% of the area of the overall emission spectrum.

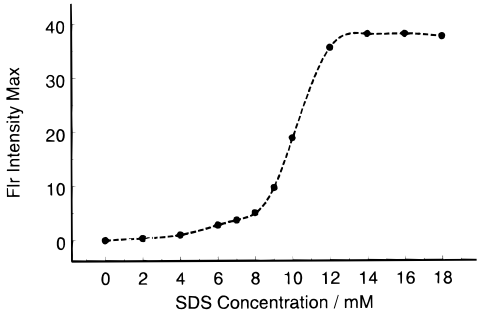

Figure 1. The variation in the maximum Prodan fluorescence intensity (excitation wavelength of 340 nm, 5 μM Prodan) as SDS concentration is increased over the range of 0−18 mM.

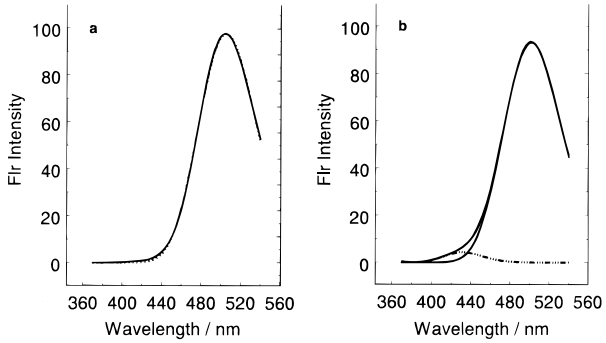

Figure 2. (a) Resolution of the overall Prodan emission spectrum for SDS micelles at 15 mM SDS and excitation λ = 360 nm. Deconvolution of the spectrum into a single Gaussian curve centered at 505 nm is illustrated. (b) Resolution of the overall Prodan emission spectrum for SDS micelles (2 mM SDS) with 0.75 M added NaCl ([Prodan] = 5 μM and excitation λ = 340 nm). Two overlapping Gaussian curves with centers at 501 and 431 nm and % areas of 95 and 5%, respectively, contribute to the overall spectrum. For both figures, the experimental emission spectrum and the theoretical fit to the experimental curve from the sum of the contributing Gaussian components are superimposed.

(b) Resolution of Prodan Fluorescence in C_nTAB (Cationic) Aqueous Micelles. For an excitation wavelength of 360 nm, the center and area of each Gaussian component resolved for Prodan in aqueous C_nTAB micelles are summarized in Table 1. Variable amounts of free Prodan (emission λ_{max} at 520−525 nm) are observed. Three major emission bands are attributed to Prodan associated with C_nTAB micellar structures, located at 493−495, 463−466, and 438−442 nm. Figures 3a and b illustrate the deconvolution of the emission spectra for 5 μM Prodan in solutions of 30.0 mM DTAB (n = 12) and 3.0 mM CTAB (n = 16), respectively. We tested the effect of addition of up to 0.50 M NaCl on 30.0 mM DTAB micellar solutions, potentially reducing the electrostatic repulsions between cationic headgroups prior to the addition of Prodan. This treatment lowered the total fluorescence intensity (for

TABLE 1: Prodan Fluorescence Emission in C_nTAB Aqueous Micelles:[a] Emission λ_{max}[b] and % Areas[c] of Gaussian Peaks Resolved by PeakFit

surfactant, *n* value	C#1	C#2	C#3	C#4
DTAB, $n = 12$	525	495	464	442
	11.2	69.1	13.2	6.5
MTAB, $n = 14$	525	495	463	438
	10.6	71.5	14.2	3.6
CTAB, $n = 16$	522	493	466	440
	18.5	56.1	18.9	6.4
OTAB, $n = 18$	520	493	464	440
	29.1	52.4	13.7	4.8

[a] Emission characteristics presented are the centers (i.e., emission λ_{max} values) in nm (first line) and % areas (second line) of Gaussian curves resolved from the overall fluorescence emission spectrum. Emission data correspond to excitation $\lambda = 360$ nm. [b] Uncertainties of ± 1 nm. [c] Uncertainties of $\pm 0.5\%$.

TABLE 2: Prodan Fluorescence Emission as a Function of pH Value[a] in LDAO Micelles: Emission λ_{max}[b] and % Areas[c] of Gaussian Peaks Resolved by PeakFit

	C#1		C#2		C#3	
pH	λ_{max}	% area	λ_{max}	% area	λ_{max}	% area
5.12	509	81.4	458	12.2	425	6.4
5.66	508	83.2	456	11.0	424	5.8
6.11	508	81.9	455	12.1	424	6.0
6.95	502	93.0			430	7.0
8.15	505	88.3			432	11.7
9.30	505	87.6			432	12.4
9.66	502	89.9			429	10.0
10.45	504	86.8			430	13.2

[a] Emission characteristics presented are the centers (i.e., emission λ_{max} values) in nm (first line) and % areas (second line) of Gaussian curves resolved from the overall fluorescence emission spectrum. Emission data correspond to excitation $\lambda = 360$ nm. [b] Uncertainties of ± 1 nm. [c] Uncertainties of $\pm 0.5\%$.

example, ratio of intensities at λ_{max} of 495 nm = 0.8 with and without 0.50 M NaCl, respectively) but had no effect on the Gaussian composition of the overall spectrum (results not shown).

(c) Resolution of Prodan Fluorescence in LDAO (Zwitterionic) Aqueous Micelles. Table 2 summarizes the Gaussian peaks resolved in the overall fluorescence spectra acquired for Prodan-incorporated LDAO micelles in aqueous solutions of varying pH at an excitation wavelength of 360 nm. At those pH values examined at or below 6.11, three Gaussian components were resolved at average λ_{max} values of 508, 456, and 424 ± 1 nm and average % area contributions of 82, 12, and 6%, respectively. In solutions of higher pH, the fluorescence spectra could be deconvoluted to yield only two overlapping Gaussian peaks at average emission λ_{max} values of 504 ± 2 nm and 431 ± 1 nm. These components contribute 89 and 11% of the total area of the fluorescence emission spectrum, respectively. Figure 4 compares the Gaussian deconvolution of the fluorescence spectra obtained at pH 6.11 and pH 6.95, illustrating the absence of the 456-nm component at higher pH.

(d) Resolution of Prodan Fluorescence in $C_{12}E_8$ and $C_{14}E_8$ (Nonionic) Aqueous Micelles. The deconvoluted fluorescence spectra of Prodan in the nonionic micelles of $C_{12}E_8$ and $C_{14}E_8$ are comprised of two Gaussian components. The peaks are centered at 498 ± 1 nm and 431 ± 2 nm in $C_{12}E_8$ micelles with % area contributions to the overall spectrum of 93 and 7, respectively. The corresponding Gaussian parameters in $C_{14}E_8$ micelles are λ_{max} at 503 ± 1 nm and 429 ± 2 nm with % area contributions of 96 and 4%, respectively. Figure 5 presents the total and deconvoluted spectra obtained with an excitation wavelength of 360 nm for (a) 4.0×10^{-4} M $C_{12}E_8$ solutions and (b) 1.0×10^{-4} M $C_{14}E_8$ solutions.

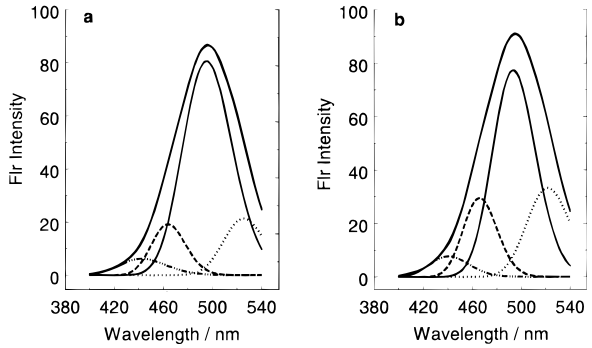

Figure 3. (a) The deconvolution of the emission spectrum for 5 μM Prodan in a solution of 30.0 mM DTAB at an excitation wavelength of 360 nm. Four overlapping Gaussians are resolved with centers at 525, 495, 464, and 442 nm and % areas of 11.2, 69.1, 13.2, and 6.5, respectively. (b) The deconvolution of the emission spectrum for 5 μM Prodan in a solution of 3.0 mM CTAB at an excitation wavelength of 360 nm. Four overlapping Gaussians are resolved with centers at 522, 493, 466, and 440 nm and % areas of 18.5, 56.1, 18.9, and 6.4, respectively. For both figures, the experimental emission spectrum and the theoretical fit to the experimental curve from the sum of the contributing Gaussian components are superimposed.

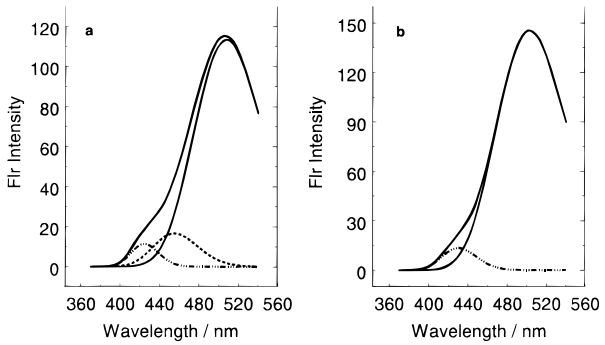

Figure 4. A comparison of the Gaussian deconvolution of the fluorescence spectra obtained for LDAO micelles at (a) pH 6.11 and (b) pH 6.95. At pH 6.11, three overlapping Gaussian curves are resolved with centers at 508, 455, and 424 nm and corresponding % area contributions of 81.9, 12.1, and 6.0%, respectively. At pH 6.95, only two Gaussian components are observed with centers at 502 and 430 nm and % area contributions of 93.0 and 7.0%, respectively. For both figures, the experimental emission spectrum and the theoretical fit to the experimental curve from the sum of the contributing Gaussian components are superimposed.

(e) Resolution of Prodan Fluorescence in Water/AOT/*n*-Heptane (Anionic) Reverse Micelles. As revealed in previous studies[2] of AOT reverse micelles, Prodan fluorescence emission spectra exhibit a dependence on the R (=[H_2O]/[AOT]) value of the surfactant preparation. Figure 6 portrays the emission spectra for AOT reverse micelles with 0.100 M AOT and R values of 2 and 40. The parameters of the Gaussian peaks extracted from the spectra using PeakFit are presented in Table 3 for R values of 2, 8, 12, 15, 20, 30, and 40. As previously observed, up to five Prodan fluorescence emission components are present. For R values of 15−40, where all five components are present in relatively constant amounts, the average centers of the Gaussian components are 514, 488, 442, 412, and 388 ± 1 nm with average % area contributions of 15, 26, 29, 21, and 9%, respectively. In general, the contribution of the 514-nm component increases with R value (and is not present at $R = 2$), while the 412-nm component decreases dramatically in % area as R increases.

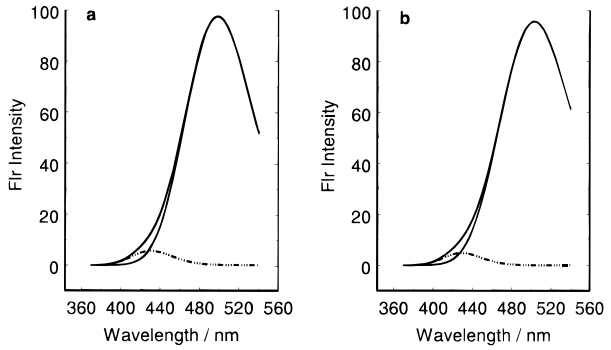

Figure 5. The total and deconvoluted Prodan fluorescence emission spectra obtained with an excitation wavelength of 360 nm for (a) 4.0×10^{-4} M $C_{12}E_8$ solutions and (b) 1.0×10^{-4} M $C_{14}E_8$ solutions. The peaks are centered at 498 and 431 nm in $C_{12}E_8$ micelles with % area contributions to the overall spectrum of 95 and 5%, respectively. The corresponding Gaussian parameters in $C_{14}E_8$ micelles are λ_{max} at 503 and 429 nm with % area contributions of 96% and 4%, respectively. For both figures, the experimental emission spectrum and the theoretical fit to the experimental curve from the sum of the contributing Gaussian components are superimposed.

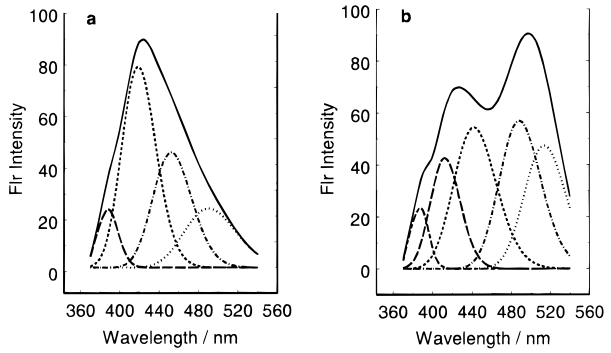

Figure 6. (a) Resolution of the overall Prodan emission spectrum for AOT/*n*-heptane/H_2O reverse micellar systems with $R = 2$, [AOT] = 0.100 M, and excitation $\lambda = 360$ nm. Four overlapping Gaussian curves with centers at 490, 453, 419, and 388 nm and % areas of 15.0, 27.0, 48.5, and 9.5, respectively, contribute to the overall spectrum. The experimental emission spectrum and the theoretical fit to the experimental curve from the sum of the contributing Gaussian components are superimposed. (b) Resolution of the overall Prodan emission spectrum for AOT/*n*-heptane/H_2O reverse micellar systems with $R = 40$, [AOT] = 0.100 M, and excitation $\lambda = 360$ nm. Five overlapping Gaussian curves with centers at 513, 488, 442, 412, and 387 nm and % areas of 17.3, 25.5, 30.8, 19.4, and 7.0, respectively, contribute to the overall spectrum. The experimental emission spectrum and the theoretical fit to the experimental curve from the sum of the contributing Gaussian components are superimposed.

(f) Resolution of Prodan Fluorescence in Water/DTAB/n-Hexanol/*n*-Heptane Reverse Micelles. In contrast to AOT reverse micelles, little variation in emission spectral shape is observed for the overall fluorescence emission spectrum of Prodan in DTAB reverse micelles (0.015 M DTAB) for *R* values between 0 and 30. Table 4 summarizes the maximal emission wavelengths and the area of each Gaussian component resolved for Prodan in DTAB reverse micelles of varying *R* value and at fixed excitation wavelength. In these systems, six major Prodan fluorescence components are observed at average λ_{max} values of 399, 420, 437, 460, 489, and 513 nm (all uncertainties ± 1 nm except 513 ± 3 nm). The dominant component in all spectra is the 460-nm Gaussian peak. Figure 7a illustrates the resolution of the overall Prodan emission spectrum into the contributing Gaussian components for reverse micelles with $R = 15$.

TABLE 3: Prodan Fluorescence Emission[a] in AOT/*n*-Heptane/H_2O Reverse Micelles[b] of Varying *R*: Emission λ_{max} and % Areas of Gaussian Peaks Resolved by PeakFit

R	C#1	C#2	C#3	C#4	C#5
2		490	453	419	388
		15.0	27.0	48.5	9.5
8	517	489	452	418	388
	9.4	24.8	21.3	35.0	9.6
12	520	490	442	411	387
	9.8	27.7	29.8	22.6	10.0
15	513	487	442	412	388
	13.8	22.6	27.5	22.8	11.6
20	515	488	442	411	389
	15.1	22.6	28.4	21.6	12.2
30	514	487	442	413	387
	14.9	30.6	28.6	19.9	6.0
40	513	488	442	412	387
	17.3	25.5	30.8	19.4	7.0

[a] Emission characteristics presented are the centers (i.e., emission λ_{max} values) in nm (first line) with uncertainties of ± 1 nm and % areas (second line) with uncertainties of ± 0.5% of Gaussian curves resolved from the overall fluorescence emission spectrum. Emission data correspond to excitation $\lambda = 360$ nm. [b] AOT reverse micelles prepared with 0.100 M AOT.

TABLE 4: Prodan Fluorescence Emission[a] in DTAB/*n*-Heptane/1-Hexanol/H_2O Reverse Micelles[b] of Varying *R*: Emission λ_{max} and % Areas of Gaussian Peaks Resolved by PeakFit

R	C#1	C#2	C#3	C#4	C#5	C#6
1	514	490	460	436	419	398
	6.9	12.3	46.6	12.6	15.4	6.2
7.5	518	490	460	437	421	399
	7.4	16.7	42.0	10.6	16.7	6.6
15	515	489	460	436	419	399
	7.4	18.0	43.4	12.7	12.2	6.3
22.5	511	488	459	436	420	401
	8.4	18.1	41.6	13.0	11.6	7.4
30	507	488	461	438	420	398
	9.1	16.2	38.4	16.1	15.0	5.2

[a] Emission characteristics presented are the centers (i.e., emission λ_{max} values) in nm (first line, ± 1 nm) and % areas (second line, ± 0.5%) of Gaussian curves resolved from the overall fluorescence emission spectrum. Emission data correspond to excitation $\lambda = 360$ nm. [b] DTAB reverse micelles prepared with 0.015 M DTAB.

(g) Resolution of Prodan Fluorescence in Water/CTAB/n-Hexanol/*n*-Heptane Reverse Micelles. The overall fluorescence emission spectrum of Prodan in CTAB reverse micelles ([CTAB] = 0.015 M) as a function of emission wavelength and *R* value is illustrated in Figure 8. Table 5 summarizes the maximal emission wavelengths and the area of each Gaussian component resolved for Prodan in CTAB reverse micelles of varying *R* value and at a fixed excitation wavelength of 360 nm. In these systems, six major Prodan fluorescence components are observed at average λ_{max} values of 397, 416, 435, 460, 490, and 514 ± 1 nm. The 514-nm component increases significantly in contribution, primarily at the expense of the 490-nm component, as the size of the water pool increases. In all cases, however, just as observed for the DTAB reverse micelles, the 460-nm component dominates the emission spectrum. Figure 7b illustrates the resolution of the overall Prodan emission spectrum into the contributing Gaussian components for reverse micelles with $R = 10$.

Discussion

To facilitate analysis, Table 6 summarizes the average λ_{max} values of the Gaussian curves comprising the overall Prodan fluorescence emission spectrum in the aqueous and reverse

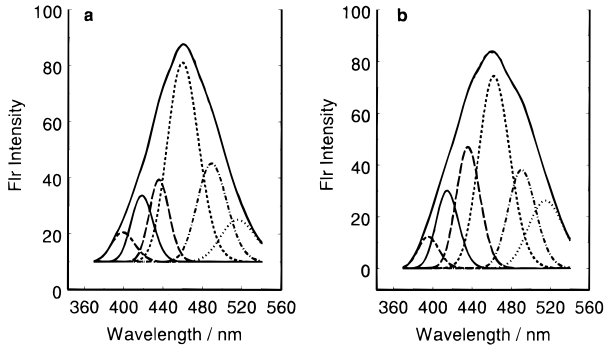

Figure 7. (a) Resolution of the overall Prodan emission spectrum for DTAB/*n*-heptane/1-hexanol/H_2O reverse micellar systems with $R = 15$, [DTAB] = 0.015 M, and excitation $\lambda = 360$ nm. Six overlapping Gaussian curves with centers at 515, 489, 460, 436, 419, and 399 nm and % areas of 7.4, 18.0, 43.4, 12.7, 12.2, and 6.3, respectively, contribute to the overall spectrum. The experimental emission spectrum and the theoretical fit to the experimental curve from the sum of the contributing Gaussian components are superimposed. (b) Resolution of the overall Prodan emission spectrum for CTAB/*n*-heptane/1-hexanol/H_2O reverse micellar systems with $R = 10$, [CTAB] = 0.015 M, and excitation $\lambda = 360$ nm. Six overlapping Gaussian curves with centers at 515, 490, 462, 435, 414, and 395 nm and % areas of 10.8, 14.7, 36.3, 19.7, 13.1, and 5.4, respectively, contribute to the overall spectrum. The experimental emission spectrum and the theoretical fit to the experimental curve from the sum of the contributing Gaussian components are superimposed.

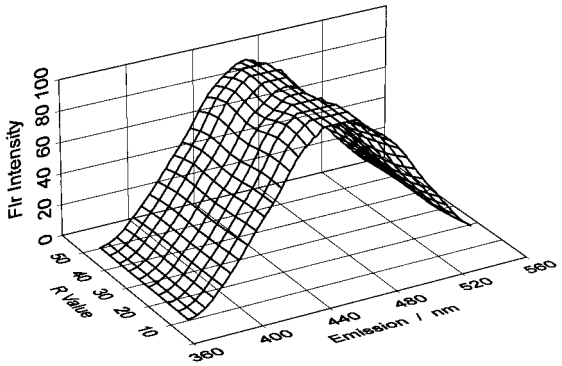

Figure 8. The overall fluorescence emission spectrum of Prodan in CTAB reverse micelles (0.015 M CTAB) as a function of emission wavelength and *R* value.

TABLE 5: Prodan Fluorescence Emission[a] in CTAB/*n*-Heptane/1-Hexanol/H_2O Reverse Micelles[b] of Varying *R*: Emission λ_{max} and % Areas of Gaussian Peaks Resolved by PeakFit

R	C#1	C#2	C#3	C#4	C#5	C#6
10	515	490	462	435	414	395
	10.8	14.7	36.3	19.7	13.1	5.4
20	512	489	460	436	417	398
	11.2	12.1	40.2	15.4	13.6	7.5
30	514	491	460	434	416	396
	10.2	8.8	50.0	9.8	14.8	6.4
40	514	490	459	435	417	396
	17.7	2.4	48.4	10.0	15.0	6.5
50	514	489	458	435	418	398
	21.3	1.7	46.1	9.4	14.3	7.4

[a] Emission characteristics presented are the centers (i.e., emission λ_{max} values) in nm (first line, ±1 nm) and % areas (second line, ±0.5%) of Gaussian curves resolved from the overall fluorescence emission spectrum. Emission data correspond to excitation $\lambda = 360$ nm. [b] CTAB reverse micelles prepared with 0.015 M CTAB.

micelles investigated. A consideration of the noncovalent interactions dictating Prodan partitioning aids in the assignment of each Prodan microenvironment.

TABLE 6: Summary of Gaussian Fluorescence Emission λ_{max}[a] Values for Prodan Incorporated in Aqueous and Reverse Micelles

aqueous micellar system	C#1	C#2	C#3
SDS	505		
SDS + 0.05 M NaCl	506		
SDS + 0.75 M NaCl	501		435
C_nTAB[b]	494	464	440
C_{12}TAB (DTAB) + 0.50 M NaCl	495	466	443
LDAO, pH 5	509	458	425
LDAO, pH 8	505		432
$C_{12}E_8$	498		431
$C_{14}E_8$	503		429

reverse micellar system	C#1	C#2	C#3	C#4	C#5	C#6
AOT/heptane/water[c]	514	488		442	412	388
DTAB/heptane/hexanol/water[d]	513	489	460	437	420	399
CTAB/heptane/hexanol/water[e]	514	490	460	435	416	397

[a] λ_{max} (center of Gaussian peak) in nm. [b] Averaged over C_nTAB systems with $n = 12$, 14, 16, and 18. A Gaussian component centered at an average value of 523 nm was resolved in all spectra and attributed to the presence of "free" Prodan not associated with the micellar structure. [c] Averaged for reverse micelles with *R* values from 12 to 40. [d] Averaged for reverse micelles with *R* values from 1 to 30. [e] Averaged for reverse micelles with *R* values from 10 to 50.

Prodan Distribution in Aqueous Micelles. In anionic and nonionic micelles, such as those composed of the surfactants SDS, $C_{12}E_8$, and $C_{14}E_8$, the nonionic and hydrophobic character of Prodan would be expected to promote a hydrophobic interaction with the alkyl tails of the micellar core and/or a nonspecific dipolar interaction with the micellar surface. The microenvironments of these two regions differ considerably in terms of polarity and water accessibility and should give rise to distinct emission λ_{max}. The Gaussian component centered at 501−506 nm in both the untreated and NaCl-treated SDS micelles reasonably corresponds to Prodan situated at the micellar surface via weak dipole interactions with the surfactant headgroups. The small shift in emission λ_{max} from that observed in aqueous solution ($\lambda_{max} = 522$ nm)[1] is consistent with this assignment. The presence of a comparable 498−503-nm component in the nonionic $C_{12}E_8$ and $C_{14}E_8$ micelles and a 505−509 nm Gaussian in the Prodan emission spectra in zwitterionic micelles also supports the assignment of this fluorescence component to Prodan situated at the micellar surface via a nonspecific dipolar interaction with surfactant headgroups. A parallel assignment of the 493−495-nm Prodan Gaussian component resolved in cationic C_nTAB micelles can be made. As previously noted,[1] the 10-nm difference in Prodan emission wavelengths for SDS and DTAB micelles most likely reflects the relative extent of water accessibility of the Prodan environments. An enhanced polarity of the SDS surfactant−water interface can be attributed to greater water penetration, in general agreement with the observation that micelles with anionic sulfate headgroups (e.g., SDS) are usually found to be more hydrated than those with trimethylammonium headgroups (e.g., DTAB).[13]

In contrast, the central core of an aqueous micelle, comprised of surfactant hydrocarbon tails, would be a considerably more nonpolar microregion with limited water accessibility. Such an environment would be expected to induce a significant blue shift in the Prodan emission λ_{max}.[1−3] The 435-nm component resolved in the NaCl-treated cylindrical SDS micelles, the 429−431-nm component in the nonionic $C_{12}E_8$ and $C_{14}E_8$ micelles, the 425−432 nm peak in the zwitterionic LDAO micelles, and the 438−442-nm component in the cationic C_nTAB micelles are attributed to Prodan molecules incorporated within the micellar core.

The 464-nm component observed in C_nTAB micelles is consistent with emission from Prodan residing in a more surfactant-intercalated domain (i.e., a more nonpolar region) than the micellar surface but not as hydrophobic as the micellar core. A strong interaction of the aromatic probe at the cationic surfactant headgroups would be a reasonable origin for the new partitioning site. Indeed, an association of aromatic compounds with the cationic headgroups on the surface of micelles composed of alkyltrimethylammonium bromide surfactants has long been speculated.[11,14−19] The presence of the 458-nm component in zwitterionic micelles at low pH (where the protonated surfactant has essentially cationic character) also corroborates the proposal of an interaction of probe and cationic headgroup. The strength of the proposed interaction is reflected in the inability of added chloride to displace the Prodan in cationic C_nTAB micelles, as revealed by the lack of change in the extent of contribution of the 464-nm component to the overall fluorescence spectrum. A cation−π interaction, with aromatic fluorophore as guest and cation as host, is a viable contributing factor to the proposed solute localization.

Prodan Distribution in Reverse Micelles. The ternary system of surfactant AOT/heptane/water leads to the formation of reverse micelles. This double-chain anionic surfactant aggregates with the polar headgroups of the amphiphiles directed toward the aqueous micellar core and the hydrophobic surfactant tails extended into the organic bulk phase. The observed behavior of Prodan fluorescence in water/AOT/*n*-heptane mixtures is consistent with the premise that Prodan partitions into multiple environments within the reverse micelles, specifically the bulk hydrocarbon continuum, the AOT interface of surfactant tails, the bound water interface at the AOT headgroups, and the inner bulk water pool. As noted in previous studies,[2] fluorescence emission from Prodan in the heptane bulk solvent is observed at an average λ_{max} of 412 nm. A minor fluorescence component at 398 nm is also attributed to emission from Prodan in the apolar medium and arises from another $\pi \rightarrow \pi^*$ transition in the absorption spectrum that is closely spaced to the 412-nm transition.[2,20] Fluorescence with an emission λ_{max} typically near 442 nm is assigned to Prodan in the surfactant interfacial region, analogous to the 425−440-nm components observed in aqueous micelles. Hydrophobic interactions principally dictate this partitioning site. Fluorescence from Prodan molecules located in the region of "bound" water immobilized via hydration of the AOT sodium counterions and ionized sulfosuccinate headgroups is ascribed to a longer wavelength component, detected near 488 nm. An even longer wavelength component, with an average λ_{max} of 514 nm, is associated with emission from Prodan molecules deep within the "free" water pool.

The major Prodan fluorescence components observed in the DTAB and CTAB reverse micellar systems can be assigned in a similar fashion. The 416−420 nm emission corresponds to Prodan in the heptane bulk solvent with some solubilized *n*-hexanol shifting the λ_{max} (from 402 nm for pure *n*-heptane[1]) to reflect a slightly more polar environment. Again, a minor fluorescence component at 398 nm is also attributed to emission from Prodan in the apolar medium and arises from another $\pi \rightarrow \pi^*$ transition in the absorption spectrum that is closely spaced to the 416-nm transition.[2,20] The 489- and 514-nm components correspond to Prodan in the bulk and free water pools, as previously observed in the AOT reverse micelles.[2]

The remaining 460-nm Gaussian resolved in C_nTAB reverse micelles is attributed to Prodan at the perimeter of the bound water layer/C_nTAB headgroup interface. The similarity of this λ_{max} value to that observed in cationic C_nTAB aqueous micelles and zwitterionic LDAO micelles at low pH further supports our proposed location. The insensitivity of this λ_{max} to *R* value would suggest a strong electrostatic association of the aromatic moiety for the quaternary ammonium cationic headgroup. A cation−π interaction is a likely contributor to the affinity of Prodan for the C_nTAB headgroups. The cation−π associations may originate from two distinct orientations of the aromatic electron π cloud relative to the cationic surfactant headgroups, via a parallel orientation in which the aromatic guest resides in a more surfactant-intercalated domain or via a tangential orientation where the aromatic residue is positioned at the perimeter of the bound water layer of the reverse micelle. Spectroscopic evidence for a dual-site mode of interaction of aromatic residues and cationic species has previously been presented.[17−19]

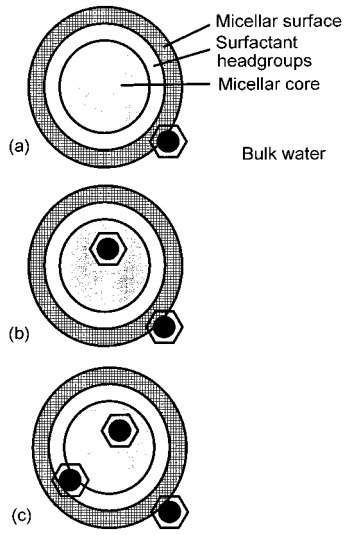

Figure 9. (a) The proposed sole site for Prodan in anionic aqueous micelles − at the micellar surface. (b) The two distribution sites of Prodan, at the micellar surface and deep within the surfactant layer, attributed to anionic micelles with added counterions that reduce headgroup repulsion and induce a cylindrical micellar shape, to nonionic micelles, and to zwitterionic micelles at high pH. (c) The three positions of Prodan—at the micellar surface, at the surfactant headgroups, and within the surfactant layer—proposed in cationic aqueous micelles and in zwitterionic micelles at low pH.

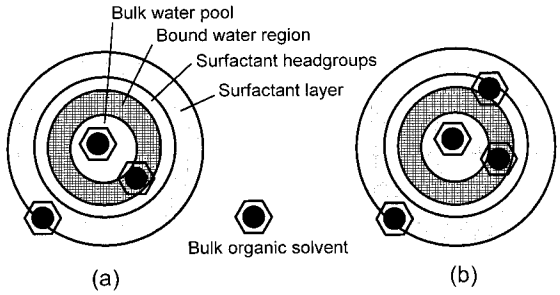

Figure 10. (a) The proposed distribution of Prodan in the anionic reverse micelles of AOT—in the free water pool, the bound water layer, the surfactant layer, and the bulk organic medium. (b) The proposed sites of Prodan in the cationic reverse micelles of DTAB and CTAB—in the free water pool, in the bound water layer, at the surfactant headgroups, in the surfactant layer, and in the bulk organic medium.

Figures 9 and 10 summarize the proposed sites of Prodan distribution within the aqueous and reverse micelles examined. Figure 9a depicts the proposed sole site for Prodan in anionic aqueous micelles—at the micellar surface. The distribution illustrated in Figure 9b, with two Prodan sites at the micellar surface and deep within the surfactant layer, is attributed to anionic micelles with added counterions that reduce headgroup repulsion and induce a cylindrical micellar shape, to nonionic micelles, and to zwitterionic micelles at high pH. The three

positions of Prodan in Figure 9c—at the micellar surface, at the surfactant headgroups, and within the surfactant layer—are the proposed sites for this aromatic probe in cationic aqueous micelles and in zwitterionic micelles at low pH. Figure 10a illustrates the proposed distribution of Prodan in the anionic reverse micelles of AOT, with the free water pool, the bound water layer, the surfactant layer, and the bulk organic medium as potential sites for the fluorophore. The additional location of Prodan at the surfactant headgroups within the cationic reverse micelles of DTAB and CTAB is the fifth site proposed in Figure 10b.

Conclusion

These spectroscopic investigations suggest a fluorescence analysis technique that can be used to ascribe multiple partitioning sites and the noncovalent forces that mediate solute partitioning within aqueous and reverse micellar systems. In particular, the expected targeting of Prodan for more specific (and hence a more limited number of) sites within aqueous micellar systems facilitates the analysis of the complex emission spectra obtained for Prodan distribution within reverse micelles. Electrostatic, dipolar, and hydrophobic interactions are attributed as the dominant "driving forces" for probe partitioning. However, while much of the focus on cation$-\pi$ interactions in aqueous media has ascribed the role of "host" to the aromatic system and "guest" to the aqueous cation, we believe that the analogous cationic "host"−aromatic "guest" interaction can be an equally significant contributor to the partitioning of aromatic solutes in supramolecular systems. Our current investigations seek further indications of the role of cation$-\pi$ interactions in the distribution of aromatic species within surfactant aggregations in both aqueous and apolar media.

Acknowledgment. This research was supported in part by a grant from the National Science Foundation Research Experiences for Undergraduates Program (Grant CHE-9322804) and by a National Institutes of Health Academic Research Enhancement Award. Acknowledgment is made to the donors of the Petroleum Research Fund, administered by the American Chemical Society, for the partial support of this research. K.K.K. also acknowledges support from a Henry Dreyfus Teacher-Scholar Award.

References and Notes

(1) Karukstis, K. K.; Suljak, S. W.; Waller, P. J.; Whiles, J. A.; Thompson, E. H. Z. *J. Phys. Chem.* **1996**, *100*, 11125.

(2) Karukstis, K. K.; Frazier, A. A.; Martula, D. S.; Whiles, J. A. *J. Phys. Chem.* **1996**, *100*, 11133.

(3) Weber, G.; Farris, F. J. *Biochemistry* **1979**, *18*, 3075.

(4) Dougherty, D. A.; Stauffer, D. A. *Science* **1990**, *250*, 1558.

(5) Kumpf, R. A.; Dougherty, D. A. *Science* **1993**, *261*, 1708.

(6) Kearney, P. C.; Mizoue, L. S.; Kumpf, R. A.; Forman, J. E.; McCurdy, A.; Dougherty, D. A. *J. Am. Chem. Soc.* **1993**, *115*, 9907.

(7) Dougherty, D. A. *Science* **1996**, *271*, 163.

(8) Mecozzi, S.; West, Jr.; A. P.; Dougherty, D. A. *J. Am. Chem. Soc.* **1996**, *118*, 2307.

(9) Ma, J. C.; Dougherty, D. A. *Chem. Rev.* **1997**, *97*, 1303.

(10) Bunton, C. A. In *Reaction Kinetics in Micelles*; Cordes, E. H., Ed.; Plenum Press: New York, 1973.

(11) Bunton, C. A. and Minch, M. J. *J. Phys. Chem.* **1974**, *78*, 1490.

(12) Hiemenz, P. C. *Principles of Colloid and Surface Chemistry*, 2nd ed.; Marcel Dekker: New York, 1986; Chapter 8.

(13) Hayter, J. B. In *Physics of Amphiphiles: Micelles, Vesicles and Microemulsions*, V. Degiorgio, Ed.; Elsevier Science: New York, 1985; pp 59−93.

(14) Bunton, C. A., Minch, M. J., Hidalgo, J., Sepulveda, L. *J. Am. Chem. Soc.* **1973**, *95*, 3262.

(15) Underwood, A. L.; Anacker, E. W. *J. Phys. Chem.* **1984**, *88*, 2390.

(16) Bachofer, S. J.; Simmonis, U.; Nowicki, T. A. *J. Phys. Chem.* **1991**, *95*, 480.

(17) Imae, T.; Kohsaka, T. *J. Phys. Chem.* **1992**, *96*, 10030.

(18) Cassidy, M. A.; Warr, G. G. *J. Phys. Chem.* **1996**, *100*, 3237.

(19) Kreke, P. J.; Magid, L. J.; Gee, J. C. *Langmuir* **1996**, *12*, 699.

(20) Nowak, W.; Adamczak, P.; Balter, A.; Sygula, A. *J. Mol. Struct.* **1986**, *139*, 13.